# Low-temperature phases of Xe on Pd(111)

J.F. Zhu,* H. Ellmer,† H. Malissa,‡ T. Brandstetter, D. Semrad, and P. Zeppenfeld§
*Institut für Experimentalphysik, Johannes Kepler Universität Linz, A-4040 Linz, Austria*
(Received 25 November 2002; revised manuscript received 7 March 2003; published 7 July 2003)

Low-energy electron diffraction (LEED) and temperature-programmed desorption (TPD) were used to determine the adsorption properties and the structural phase diagram of Xe on the clean Pd(111) surface. The binding energy of a Xe atom to the substrate is found to be quite strong ($320\pm10$ meV), whereas the effective Xe-Xe lateral interaction is extremely weak ($V_{lat}\leqslant 10$ meV) and most likely attractive on the clean Pd(111) surface. Within the monolayer regime, a phase transition sequence from a commensurate $(\sqrt{3}\times\sqrt{3})R30°$ phase to a hexagonal incommensurate phase (HI) and, finally, to a hexagonal incommensurate rotated phase (HIR) is observed. The resulting phase diagram is compared to theoretical predictions and other rare-gas adsorption systems. The Xe adlayer structure turns out to be extremely sensitive to the presence of impurities, such as H and CO. This sensitivity can be rationalized by the weak Xe-Xe lateral interaction.

DOI: 10.1103/PhysRevB.68.045406 PACS number(s): 68.43.Fg, 68.43.Mn, 61.14.Hg

## I. INTRODUCTION

The interactions between physisorbed particles, namely rare-gas atoms adsorbed on graphite[1] and various metal surfaces,[2] are usually described by attractive forces of the well-known van der Waals type. As a result, rare-gas adlayers have often been considered as model systems for the study of phase transitions in two dimensions.[3] Due to the attractive nature of the lateral interactions physisorbed rare gases are expected to undergo a first-order two-dimensional (2D) gas-solid phase transition and to form islands (in coexistence with a 2D gas phase) in the submonolayer regime and at low enough temperatures. On the other hand, repulsive contributions to the lateral interaction supplementing the attractive van der Waals interaction have been identified early on, and may lead to a significant reduction of the net (effective) lateral interaction.[3] These contributions arise from substrate-mediated (McLachlan) and multibody interactions as well as from the dipole-dipole repulsion between the Xe atoms that acquire a permanent polarization upon adsorption. In addition, the strain induced by the corrugation of the holding potential together with the lattice mismatch can be viewed as a repulsive effective Xe-Xe lateral interaction. In some cases, the sum of these repulsive contributions may even outweigh the attractive van der Waals interaction between the adsorbates leading to an overall lateral *repulsion*, as claimed in the case of Xe/W(110),[4] Xe/Ni(100),[5] and Xe adsorbed on various Pd surfaces.[6,7] An overall repulsive lateral interaction on Pd(111) was conjectured from the monotonic decrease of the total binding energy of a Xe atom from 360 meV at low coverage to 335 meV close to monolayer completion.[6] Furthermore, instead of forming two-dimensional islands, Xe was found to adsorb in a ''dilute'' phase up to rather high coverages.[7] Substantial repulsive contributions to the lateral interaction have been correlated with large work function changes, i.e., a large adsorption-induced dipole moment.[6]

The experimental findings suggesting a significant repulsive contribution to the Xe lateral interactions—especially on the strongly binding substrates Pt and Pd—are in agreement with density functional theorem (DFT) calculations for the rare gases adsorbed on jellium[8] as well as DFT calculations for Xe on Pt(111) (Refs. 9 and 10) and Pd(111).[10] Even more surprising, these studies predict an *on-top* adsorption site[9,10] and a very large vibration energy for an *isolated* adsorbed Xe atom on Pt(111) of about 8.5 meV (Ref. 9) as compared to the experimental value of 3.4 meV for the *dense* Xe monolayer.[11] Meanwhile, the on-top adsorption site for Xe has been confirmed experimentally on various close packed metal surfaces such as Pd(111),[12,13] Cu(111),[14] Ru(0001),[15] and Pt(111).[16] Furthermore, the correlation between adsorption strength and strong lateral repulsive contributions has been seen in the case of Xe adsorbed at step edges on the Pt(111) surface.[17,18] Whereas on Pt(111) the interaction between Xe atoms is overall repulsive only at the more strongly binding Pt step edges, the Xe-Xe interaction was assumed to be repulsive even on terraces in the case of Pd(111). The present study reveals that the repulsive contribution to the Xe-Xe lateral interaction on Pd(111) is, indeed, quite important and comparable in magnitude to the attractive van der Waals contribution. Consequently, the sum of both contributions yields a very weak *effective* lateral interaction which, however, is probably still *attractive* on the *clean* Pd(111) substrate.

Low-energy electron diffraction (LEED) and spin-polarized LEED (SPLEED) studies have revealed several different adlayer structures for Xe adsorbed on Pd(111). Up to a Xe coverage just below $\Theta=0.33$ a weakly correlated (''dilute'') phase was reported and attributed to a net repulsive interaction between the Xe atoms. For $\Theta=0.33$, the Xe adlayer forms a rather well ordered $(\sqrt{3}\times\sqrt{3})R30°$ phase.[6,7,12,19] Upon further exposure of Xe at a surface temperature $T=55$ K, additional high-order commensurate phases with large superstructure unit cells were observed, namely, a $(\sqrt{19}\times\sqrt{19})R23.4°$ phase at a coverage $\Theta=0.37$ (Refs. 12 and 19) and a $(\sqrt{7}\times\sqrt{7})R19.2°$ phase with a saturation coverage of $\Theta=0.43$.[7,19] Both phases exist in two domains rotated against each other. Also, the phase transition from $(\sqrt{3}\times\sqrt{3})R30°$ to $(\sqrt{19}\times\sqrt{19})R23.4°$ to $(\sqrt{7}\times\sqrt{7})R19.2°$ as a function of coverage was reported for Xe

 ©2003 The American Physical Society

on Pd(111).[19] The $(\sqrt{3}\times\sqrt{3})R30°$ structure can also be obtained at higher temperatures ($65\pm5$ K), whereas at 80 $\pm5$ K only the ''dilute'' phase was found to be stable against desorption. The Xe atoms in the ''dilute'' phase and in the $(\sqrt{3}\times\sqrt{3})R30°$ phase where found to reside in on-top positions.[7,13]

Kessler *et al.*[20,21] also reported an incommensurate superstructure at a coverage $\Theta=0.42$ obtained from the $(\sqrt{3}\times\sqrt{3})R30°$ structure by compressing and slight rotations by $\pm3.8°$. Starting from the $(\sqrt{7}\times\sqrt{7})R19.2°$ structure and increasing the Xe coverage at sufficiently low temperature, the formation of a Xe(111) crystal was reported by Hilgers.[19] This Xe(111) film was azimuthally aligned with the $(\sqrt{7}\times\sqrt{7})R19.2°$ structure and thus occurred in two orientations rotated by $\pm19.2°$ with respect to the Pd(111) substrate.

The first LEED intensity analysis for Xe/Pd(111) gave a binding distance in the $(\sqrt{3}\times\sqrt{3})R30°$ phase of $d=3.5\pm0.1$ Å with the Xe atoms being adsorbed in hollow sites.[12] In the ''dilute'' phase the adsorbed Xe atoms were found to occupy on-top sites with a Xe-Pd distance $d=4.0\pm0.1$ Å.[12] More recently, Caragiu *et al.*[13] found that also in the $(\sqrt{3}\times\sqrt{3})R30°$ phase Xe is adsorbed on top of the Pd atoms, with a bond length $d=3.07\pm0.06$ Å.

Contrary to the results reported previously by Hilgers *et al.*,[12] we find a number of additional phases for Xe/Pd(111) not only in the monolayer regime, but also in the bilayer and multilayer regime, depending on the substrate temperature $T$ and the Xe coverage $\Theta$. In addition, the phase diagram was found to be extremely sensitive to small impurity concentrations. In fact, the previously reported $(\sqrt{19}\times\sqrt{19})R23.4°$ and $(\sqrt{7}\times\sqrt{7})R19.2°$ phases appear to be related to residual H and CO contamination, respectively.[22] In the following, we will report the complete structural phase diagram of Xe, which we believe to be characteristic of the *clean* Pd(111) surface.

The paper is organized as follows: After a brief description of the experimental setup in the next section, we will present the phase diagram extracted from LEED patterns, LEED intensity versus exposure curves, and temperature-programmed desorption spectra. The results are discussed in the light of previous experimental work and theoretical predictions of 2D phase diagrams and phase transitions.

## II. EXPERIMENT

The experimental setup[23] consists of an ultrahigh vacuum (UHV) chamber with a base pressure in the low $10^{-11}$ mbar range. Besides a supersonic helium nozzle beam for thermal energy atom scattering (TEAS), it contains common surface analytic tools, like an Auger electron spectroscopy (AES) facility, a quadrupole mass analyzer (QMA) for temperature-programmed desorption (TPD) studies, and a video LEED system.

The sample, a hat-shaped Pd(111) crystal, is mounted on a three-axis goniometer and can be positioned with respect to the LEED beam via a 3D manipulator. The two wires of a K-type thermocouple are welded on opposite sides of the crystal to average over the temperature gradient across the sample. The sample can be cooled to 20 K by a helium flow cryostat and heated to 1200 K using a computer controlled electron impact heater.[24] After a prolonged treatment in an oxygen atmosphere of $10^{-8}$ mbar at 1000 K, the sample was finally cleaned by repeated cycles of sputtering with 800 eV $Ar^+$ ions at 620 K and consecutive flash annealing to 1000 K. The surface cleanliness was checked by TPD and LEED and the cleaning cycles were repeated until no traces of the main contaminants CO and H could be detected. The overall crystalline quality of the sample surface was checked by recording LEED images from different areas of the crystal surface.

Xe was exposed by backfilling the chamber with Xe up to a partial pressure of about $10^{-8}$ mbar for a certain period of time. The Xe pressure reading was previously calibrated against a spinning rotor gauge and only the corrected values for the Xe partial pressure and the Xe exposures are given here. The conversion between exposure (1 Langmuir = 1 L $=10^{-6}$ torr s) and coverage is determined from $I(t)$ curves (LEED spot intensity versus time), showing distinct kinks at monolayer, bilayer, and trilayer completion [see, e.g., Fig. 1(b)]. The absolute coverage $\Theta$ is defined as the number of Xe atoms per Pd(111) surface atom. For instance, the completion of the $(\sqrt{3}\times\sqrt{3})R30°$ phase at 2.9 L corresponds to $\Theta=1/3$ or a surface atom density of $5.1\times10^{14}$ Xe atoms/cm$^2$. We found no differences in the Xe adlayer structures when the LEED filament and/or the electron beam ($I_{\text{beam}}<2$ $\mu$A) were switched on or off during the preparation of the Xe adlayers. On the other hand, adsorption from the residual gas (especially hydrogen and CO) was found to have a strong influence on the Xe structures and phase transitions. In order to avoid contamination induced effects, the background pressure had to be kept below $3\times10^{-11}$ mbar during the entire experiment.

## III. RESULTS

We determined the structural phase diagram (summarized in Fig. 4) from the recorded LEED images and LEED $I(t)$ curves, by identifying different phases as a function of sample temperature $T$ and Xe coverage $\Theta$. The clean Pd(111) surface was exposed to a certain amount of Xe at a given temperature, then LEED images were recorded either with the 3D Xe gas pumped off or not. We also monitored the intensity of the (10), (01), and $\sqrt{3}$ diffraction spots as a function of Xe exposure at different temperatures. To this end, we backfilled the chamber with a certain Xe partial pressure ($\sim10^{-8}$ mbar) and followed the spot intensity corrected for the background as a function of time [$I(t)$ curves]. We set finite windows around the spots and subtracted from the total intensity inside the window the background calculated from the intensity at the window perimeter.

### A. LEED intensity curves: Xe adsorption and adlayer morphology

The intensities of the (10) and (01) LEED spots plotted as a function of the Xe exposure show distinct kinks at the completion of the first monolayer at 3.75 L [Figs. 1(a,b)]. Below 45 K the decay of the intensities with additional ex-

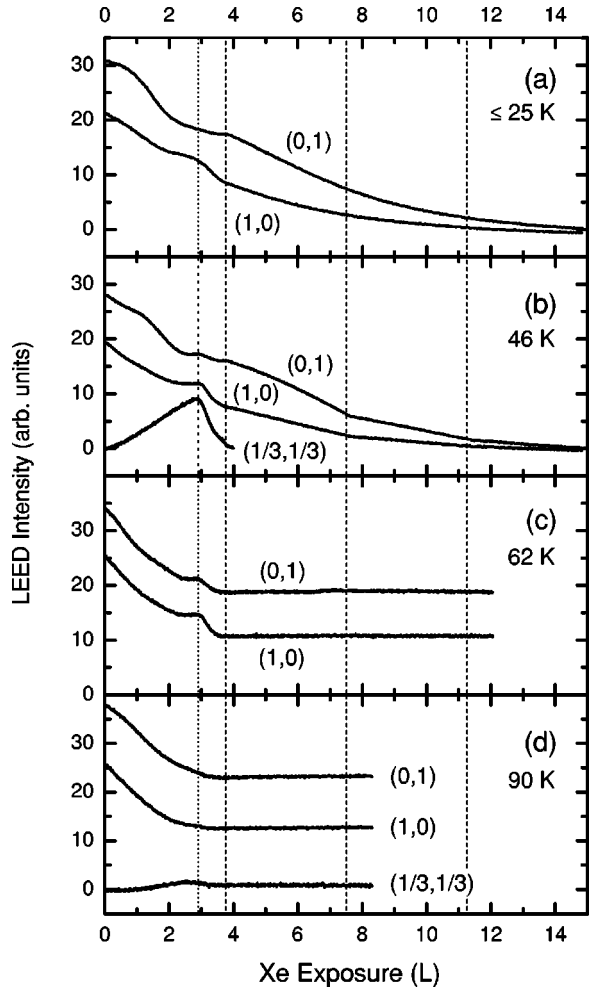


FIG. 1. Xe adsorption curves: Intensity of the (1,0) and (0,1) LEED spots of the Pd(111) substrate as a function of Xe exposure at $\lesssim$25 K (a), 46 K (b), 62 K (c), and 90 K (d); electron beam energy 60 eV; Xe partial pressure $8\times10^{-9}$ mbar. In (b) and (d) the intensity variation of the (1/3,1/3) LEED spot characteristic of a $(\sqrt{3}\times\sqrt{3})R30°$ phase is also shown. The dashed vertical lines at 3.75 L, 7.5 L, and 11.25 L, correspond to mono-, bi-, and trilayer completion, respectively. The dotted line at 2.9 L indicates the completion of the $(\sqrt{3}\times\sqrt{3})R30°$ phase ($\Theta=1/3$).

posure is roughly exponential and, therefore, the growth seems to be three dimensional [Fig. 1(a)]. For temperatures between 45 K and 60 K [Fig. 1(b)], distinct kinks can also be seen at the coverages corresponding to bi-, and trilayer completion at 7.5 L and 11.3 L, respectively, indicating layer by layer growth. Above 60 K, a second layer cannot be condensed at a typical 3D Xe partial pressure of $10^{-8}$ mbar. At temperatures between 60 K and 90 K [Figs. 1(c,d)], there only remains the shoulder in the $I(t)$ curves, which corresponds to the completion of the $(\sqrt{3}\times\sqrt{3})R30°$ phase at 2.9 L followed by an additional slight decay characteristic for a (partial) compression of the monolayer. The maximum amount of Xe adsorbed on Pd(111) at $10^{-8}$ mbar corresponds to 3.75 L at 60 K and 2.9 L at 90 K. For higher exposures, the LEED intensities remain constant.

Also shown in Fig. 1(b) is the Xe-induced (1/3,1/3) spot intensity, which rises up to a maximum at 2.9 L. This maximum corresponds to the completion of the $(\sqrt{3}\times\sqrt{3})R30°$ commensurate phase, i.e., to a coverage $\Theta=1/3$. The compression of the $(\sqrt{3}\times\sqrt{3})R30°$ phase leads to a splitting of the (1/3,1/3) spot into 3 or 6 spots. This explains the sudden decrease of the (1/3,1/3) spot intensity for $\Theta>0.33$. The constant value of 3.75 L required for the saturation of the first and all subsequent Xe layers indicates a constant sticking coefficient, if we assume that the density of the compressed monolayer is about the same as the surface density of the multilayer Xe films. Since the sticking coefficient of Xe on a Xe film can be assumed to approach unity at low surface temperature, the sticking coefficient in the monolayer regime must also be close to one. A constant sticking coefficient $s$ close to unity is also consistent with the Xe atom density $n_{Xe}$ obtained experimentally after exposing the sample for a given time interval $t$ to a Xe atmosphere (gas temperature $T_g=300$ K, partial pressure $p$) and the value calculated from kinetic gas theory $n_{Xe}=spt/\sqrt{2\pi m_{\mathrm{Xe}}k_BT}$. For instance, the calculated Xe atom density for an exposure of 2.9 L and a sticking coefficient $s=1$ amounts to $5.14\times10^{14}$ Xe atoms/cm$^2$ or $\Theta=0.34$, which is in excellent agreement with the saturation coverage $\Theta=1/3$ of the $(\sqrt{3}\times\sqrt{3})R30°$ phase. This calibration also gives the saturation coverage of the monolayer and the subsequent multilayers to be $\Theta=0.43\pm0.1$ and, hence, a Xe nearest-neighbor spacing of $4.2\pm0.1$ Å, slightly smaller than the value for bulk Xe (4.34 Å).

### B. LEED patterns: Xe adlayer structures and phase diagram

For low exposures, Xe initially forms a 2D gas phase on the surface whose saturation coverage does not exceed a few percent of a monolayer at low temperatures. We observe a decrease of intensity of the (10) and (01) spots, but no (1/3,1/3) spots [see, e.g., Fig. 1(b)]. From the LEED images, we cannot decide whether Xe adsorbs at the step edges first. With increasing exposure up to 2.9 L ($\Theta=0.33$), an ordered $(\sqrt{3}\times\sqrt{3})R30°$ LEED pattern [Fig. 2(a)] gradually develops and sharpens, indicating the formation of commensurately ordered Xe patches, whose size increases continuously with coverage. In contrast to Xe/Pt(111), this phase can already be seen at 40 K and is stable up to 80–100 K depending on the surface coverage. At temperatures above 100 K, the commensurate $(\sqrt{3}\times\sqrt{3})R30°$ phase dissolves into a 2D disordered (gas or liquid) phase and, finally, Xe completely desorbs from the surface. In the temperature range between 100 K and 104 K, the intensity of the (10) spots decreases upon adsorption, whereas the intensity of the (1/3,1/3) spots increases only slightly. For still higher temperatures the (10) spot intensity does not change upon exposure at a Xe partial pressure of the order of $10^{-8}$ mbar.

Increasing the Xe exposure to 3.75 L ($\Theta=0.43$) at 40 K $\leqslant T\leqslant$ 70 K leads to a phase transition from the commensurate $(\sqrt{3}\times\sqrt{3})R30°$ phase to a compressed incommensurate (IC) phase and, finally, to a hexagonal incommensurate rotated (HIR) phase. The LEED pattern obtained from the IC phase [Fig. 2(b)] shows the splitting of each (1/3,1/3) spot

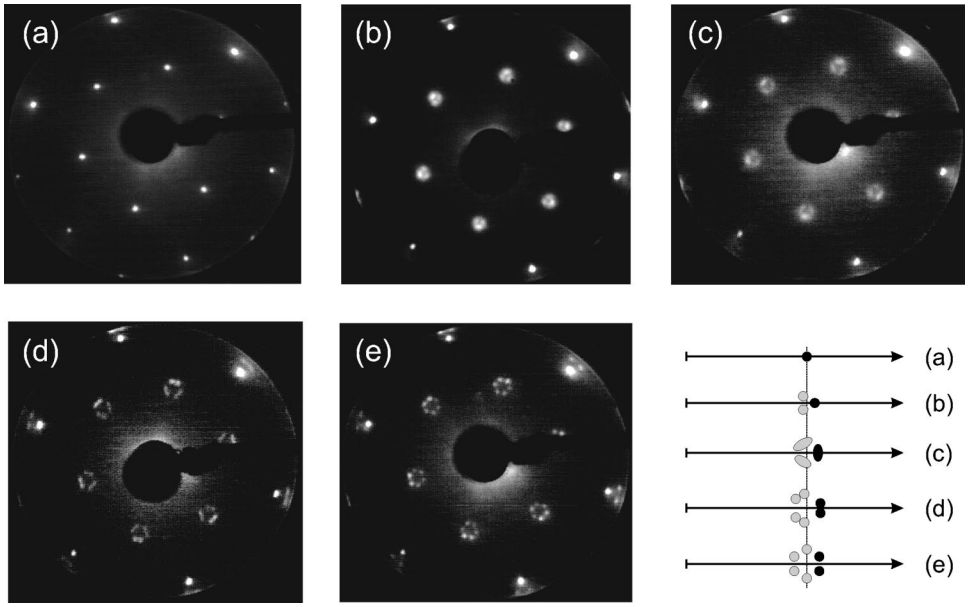


FIG. 2. Examples of LEED patterns (beam energy, 60 eV) characterizing the Xe adlayer structure in the monolayer regime as a function of coverage: (a) $(\sqrt{3}\times\sqrt{3})R30°$ phase, (b) hexagonal incommensurate phase (HI), (c) onset of the adlayer rotation, (d) and (e) hexagonal incommensurate rotated phase (HIR). The lower right panel shows a schematic of the Xe-induced spot splitting in the vicinity of the (1/3,1/3) spot position (thin vertical line). Different shades of gray symbolize the relative spot intensities.

into a spot triplet forming a triangle pointing outwards. Such a splitting is characteristic for a domain wall phase, which in the present case can be identified as a hexagonal domain wall phase with superheavy domain walls.[25] The distance of the corner spots from the center of the triangle [located at the original (1/3,1/3) position] increases with increasing coverage [Fig. 2(c)], and finally the spots at each corner of the triangle split into two new spots indicating a rotation of the Xe adlayer with respect to the Pd(111) high symmetry direction [Fig. 2(d)]. The spot splitting and rotation continue to increase until at the saturation coverage of 3.75 L the six spots of the HIR phase are clearly resolved [Fig. 2(e)].

Starting with a Xe exposure of 3.75 L at 70 K and raising the temperatures to $T=90$ K leads to a partial desorption of Xe and causes the phase transition from HIR to HI until at 90 K a sharp $(\sqrt{3}\times\sqrt{3})R30°$ LEED pattern is obtained. This reflects the fact that the compression and hence the formation of the dense domain walls are energetically unfavorable.

At still higher Xe exposures ($>3.75$ L) and for $T<60$ K, a Xe bilayer starts to grow that can be identified in the LEED pattern by the appearance of a ''seven-spot'' diffraction pattern [Fig. 3(a)]. The distance between the central spot of this seven spot arrangement and the (0,0) spot closely matches the nearest-neighbor lattice spacing of the bulk Xe(111) single crystal of $a^b_{\mathrm{Xe}}=4.34$ Å, i.e., the seven spots are no longer centered around the commensurate (1/3,1/3) position ($a^c_{\mathrm{Xe}}=4.76$ Å). The surrounding six spots can be attributed either to the double diffraction from the incommensurate Xe bilayer and the underlying Pd(111) substrate or to a periodic buckling of the bilayer in response to the substrate corrugation (Moiré pattern). In both cases the spot splitting is consistent with a misfit $m=1-a^c_{\mathrm{Xe}}/a^b_{\mathrm{Xe}}=-9\%$ and a $R30°$ azimuthal orientation of the adlayer with respect to the substrate. Upon further increase of the exposure at $T<54$ K, the second-order diffraction and/or the buckling amplitude gradually weakens and the six outer spots fade away until only single, sharp Xe(111) spots (rotated by 30° with respect to the substrate) remain [Fig. 3(b)]. Between 54 K and 60 K and for exposures higher than 3.75 L, the LEED images show six short bars (containing, most likely, two individual but unresolved spots per bar) around the central Xe(111) spots. Above 60 K and for Xe background pressures $\lesssim 10^{-8}$ mbar, only the Xe monolayer is stable against desorption and a second layer cannot be adsorbed on Pd(111).

In another series of experiments, we exposed the Pd(111) surface at 40 K and carefully annealed the adsorbed Xe layer to a given temperature, at which a LEED image was then recorded. These results are consistent with the results above and the phase diagram depicted in Fig. 4. Small differences between the constant temperature and the annealing experiments may be attributed to nonequilibrium effects, since in the latter case the ordering of the adlayer and partial desorption may occur during the annealing.

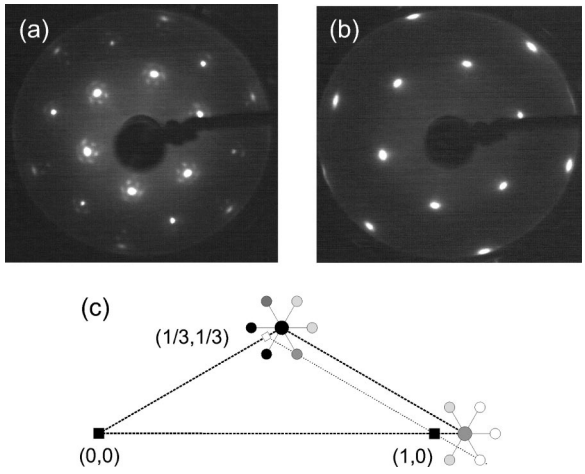


FIG. 3. (a) LEED pattern of the Xe bilayer structure (beam energy, 90 eV) and (b) LEED pattern of a multilayer Xe film (beam energy: 60 eV). (c) Schematic of the spot splitting for the Xe bilayer showing the relationship between the satellite spots, the position of the substrate spots (dark squares), and the nominal position of the (1/3,1/3) spot (small open square). Different shades of gray symbolize the relative spot intensities.

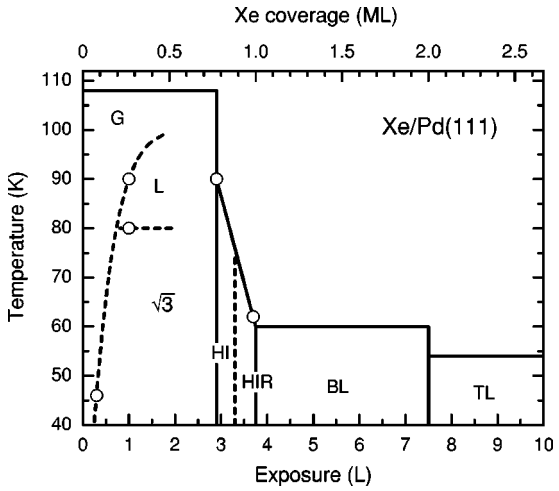


FIG. 4. Schematic structural phase diagram for Xe/Pd(111), indicating the regions of stability of the various phases. G, 2D gas phase; L, liquid phase; $\sqrt{3}$, $(\sqrt{3}\times\sqrt{3})$R30° phase; HI, hexagonal incommensurate phase; HIR, hexagonal incommensurate rotated phase; BL, bilayer; TL, trilayer. Dashed lines are rough estimates only; the upper solid lines where derived from adsorption (Fig. 1) and desorption curves (Fig. 6) and correspond to the threshold temperatures where the vapor pressure of the respective phase exceeds $\sim 10^{-8}$ mbar. Circles are data points obtained from Figs. 1 and 7.

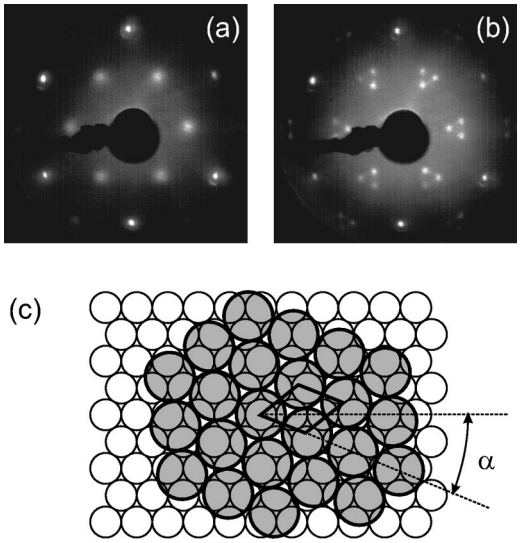


FIG. 5. Influence of surface impurities (most likely hydrogen contamination) on the phase diagram. (a) ''Dilute'' phase obtained after exposure of 0.8 L at 60 K. (b) $\gamma$ phase obtained at monolayer saturation (3.4 L) at 60 K. Electron beam energy, 101 eV. (c) Schematic view of the Xe adlayer structure in the $\gamma$ phase with coverage $\Theta = 0.40 \pm 0.01$ and rotation angle $\alpha = (22.2 \pm 1)°$, as derived from the spot splitting in (b).

### C. Influence of surface impurities

Even after careful preparation, a small residual contamination cannot be completely ruled out. If the Xe adsorption experiments were not conducted under optimum vacuum conditions and immediately after the sample preparation, we could repeatedly observe two characteristic changes in the LEED patterns and their evolution with coverage and/or temperature. (i) In many cases, the (1/3,1/3) spot of the initial $(\sqrt{3}\times\sqrt{3})R30°$ structure became diffuse over an extended coverage regime [Fig. 5(a)], which is reminiscent of the ''dilute'' phase reported in previous studies. (ii) A new phase was obtained at monolayer saturation characterized by a spot splitting into a triangle pointing *inward* as illustrated in Fig. 5(b). Sometimes, we could still observe the same sequence of the splitting of the (1/3,1/3) spot into a triangle pointing outwards (HI phase) followed by an azimuthal splitting of the 3 individual spots indicating the rotation of the adlayer (HIR phase). In contrast to the ''clean'' case, the spot rotation continued beyond the ''six-spot'' structure [Fig. 2(e)] until neighboring satellites joined again, giving rise to 3 spots forming a triangle pointing inward.

In fact, the (1/3,1/3) spot exhibits a triangular structure at coverages well below the saturation of the $(\sqrt{3}\times\sqrt{3})R30°$ phase at $\Theta = 1/3$. This could explain the diffuseness of the spot, but then the compression of the adlayer should start well below the saturation of a homogeneous $(\sqrt{3}\times\sqrt{3})R30°$ monolayer. A similar situation has been observed previously in the case of Kr on graphite,[26] where the addition of deuterium gas also lead to an early compression of the Kr 2D islands via the same transition from a commensurate $(\sqrt{3}\times\sqrt{3})R30°$ phase to a HI domain wall phase. In the present case, we believe that the modification of the Xe phase diagram on the slightly contaminated surface could be due to adsorbed hydrogen. This is supported by experiments in which well defined amounts of hydrogen were preadsorbed on the clean Pd(111) surface.[22] It was found that hydrogen exposures of the order of $10^{-2}$ L only give rise to similar characteristic features as described above: a diffuse (1/3,1/3) spot at intermediate coverages and an inward pointing triangle at monolayer saturation. The size of this triangle, i.e., the final spot splitting depends on the hydrogen coverage. At larger hydrogen precoverages (exposures $\geqslant 0.05$ L) the spots at the corners of the triangle are again split, eventually giving rise to a LEED pattern characteristic of a $(\sqrt{19}\times\sqrt{19})R23.4°$ structure.

As a result, we are confident that the phase diagram in Fig. 4 extracted from the LEED patterns in Figs. 2 and 3 is, indeed, characteristic of the *clean* Pd(111) surface. However, due to the extreme sensitivity of the Xe adlayer structure to smallest amounts of residual surface impurities, we cannot rule out that the small but finite concentration of residual surface defects or impurities, still present on the supposedly clean surface, may already influence the details of the Xe phase diagram.

### D. Temperature-programmed desorption

Complementary information on the binding energy of Xe in different layers and monolayer phases as well as on the adsorbed amount (relative coverages) in these phases have been obtained from TPD experiments. Figure 6 shows a series of TPD spectra recorded for different amounts of Xe adsorbed on the supposedly *clean* Pd(111) surface. The leading edge of the multilayer desorption peak (not shown) was used to calibrate the temperature scale.[27] From a linear fit to

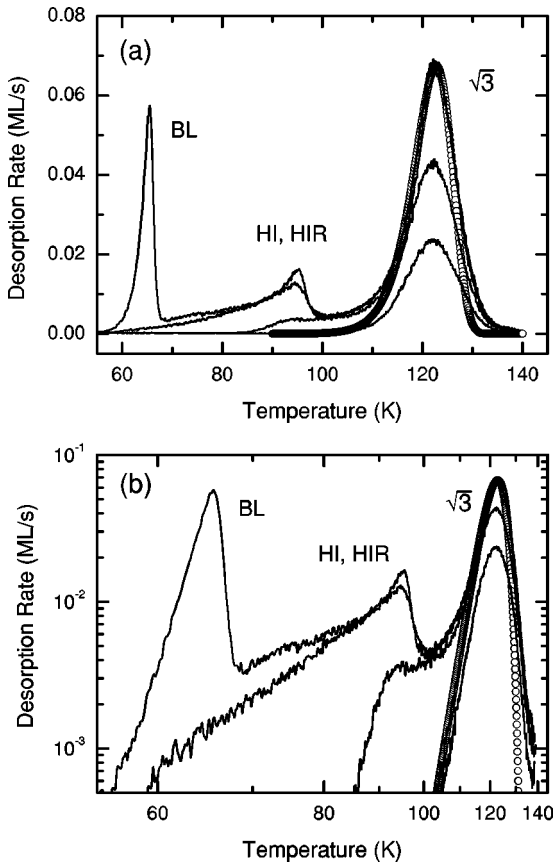


FIG. 6. Temperature-programmed desorption spectra (TPD) of Xe/Pd(111) for different initial coverages ranging between $\Theta = 0.13$ (0.3 ML) and $\Theta = 0.52$ (1.2 ML). (a) Linear representation, (b) Menzel-Schlichting plot. Small open circles indicate the ideal first-order desorption behavior, calculated by integrating the Polanyi-Wigner equation using a desorption energy $E_{des}^{0} = 320$ meV and a prefactor $\nu_0 = 5 \times 10^{12}$ Hz. Only the calculated curve for saturation coverage of the uncompressed phase ($\Theta = 1/3$) is shown.

the leading edge of the zero-order bilayer desorption peak (BL) in the ''Menzel-Schlichting'' plot [logarithmic desorption rate versus reciprocal temperature, with the $x$ axis inverted as compared to an Arrhenius plot;[27] see Fig. 6(b)] a desorption energy $E_{des}^{BL} = 176 \pm 5$ meV and a desorption prefactor $\nu_0 = 3 \times 10^{12 \pm 0.2}$ Hz is deduced. In the monolayer regime two peaks at 95 K and 122 K can be distinguished, corresponding to the compressed (HI, HIR) and the $(\sqrt{3} \times \sqrt{3})R30°$ phase, respectively. The relative area of these two desorption peaks is consistent with the Xe coverages of 1/3 (commensurate) and 0.43 (monolayer saturation) as determined from the adsorption curves (Sec. III A). The high-temperature desorption peak exhibits first-order behavior (constant peak position). Both the initial slope and a Redhead analysis give a total binding energy in this uncompressed, commensurate phase of $E_{des}^{0} = 320 \pm 10$ meV and a desorption prefactor $\nu_0 = 5 \times 10^{12 \pm 1}$ Hz. Using these values, we have calculated the first-order desorption curves by integrating the Polanyi-Wigner equation. The result for $\Theta = 1/3$ is plotted in Fig. 6 for comparison. The agreement with the experimental data is excellent for the leading edge (which is relevant for extracting $E_{des}^{0}$ and $\nu_0$), whereas an additional high-temperature ''tail'' can be seen in the experimental spectra. This tail could be due to the presence of stronger binding sites (steps, defects, impurities) or simply be an artifact due to the finite pumping speed and the accumulation of residual Xe gas starting to desorb from parts of the sample holder or cryostat.

## IV. DISCUSSION

### A. Adlayer structure and phase diagram

The phase diagram and phase transitions of the rare gases on graphite and many metal surfaces have been studied extensively both experimentally[1,2] and by theory.[3] A transition from a $(\sqrt{3} \times \sqrt{3})R30°$ phase into an incommensurate phase upon monolayer compression has been reported for Kr on graphite[28,29] and for Xe adsorbed on Pt(111).[30] Theory predicts that the transformation from the $(\sqrt{3} \times \sqrt{3})R30°$ commensurate phase (C) into a HI phase can occur either directly, via a first-order transition, or via an intermediate striped incommensurate (SI) phase.[31] In the latter case, both transitions C→SI and SI→HI are continuous. Both cases were, indeed, observed experimentally: Kr/graphite shows a C→HI transition, whereas Xe/Pt(111) presents an example for the sequence C→SI→HI. With increasing compression (large lattice misfit), the HI incommensurate adlayer may rotate as a whole to form a so called HIR phase. Such a rotation can reduce the overall strain energy of the adlayer, as was first shown by Novaco and McTague.[32] Indeed, Kr/graphite, Xe/Pt(111) and many other rare-gas systems were found to form HIR phases upon monolayer completion.

Consequently, the sequence C→HI→HIR observed for Xe on Pd(111) is quite consistent with the known behavior of the rare gases on hexagonal surfaces. Also the existence of a 2D gas phase at low coverages and a disordered (liquid) phase at higher temperatures (Fig. 4) is common to most rare-gas adlayers and physisorption systems in general. Yet, there are a few important differences between the Pd(111) and the Pt(111) case: (i) on Pd(111) the $(\sqrt{3} \times \sqrt{3})R30°$ phase is obtained already at low temperature (40 K), whereas for Pt(111) it is only stable for temperatures above 60 K. Since the nominal lattice misfit in the commensurate phase is only slightly smaller for Xe/Pd (9%) than for Xe/Pt (10%), this is a first indication for a relatively weaker lateral Xe-Xe interaction and, hence, a stronger influence of the substrate corrugation in the case of Pd(111). (ii) On Pd(111), Xe was reported to adsorb in a ''dilute'' phase with weak $\sqrt{3}$ superstructure peaks up to rather high coverage,[7] whereas on Pt(111) large islands are formed after 2D condensation, indicating a sizable attractive lateral interaction on Pt(111).[18] In contrast to the previous work, conducted at elevated temperatures, we find rather sharp (1/3,1/3) spots at intermediate coverages and lower surface temperature. On the other hand, the spot intensity and sharpness decrease steadily with increasing temperature. As an example, Fig. 7 shows the (reversible) variation of the (1/3,1/3) spot intensity for a Xe coverage of $\Theta = 0.11$, which is about one-third of

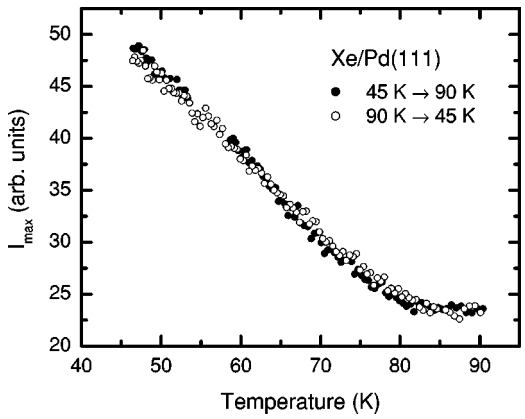


FIG. 7. Variation of the (1/3,1/3) spot intensity as a function of temperature recorded after Xe exposure of 1.0 L ($\Theta = 0.11$).

the saturation density of the $(\sqrt{3}\times\sqrt{3})R30°$ phase. In this regime, a completely disordered (''dilute'') 2D Xe phase is obtained above 80 K.[33] This behavior can again be explained in terms of *weak* lateral interactions, but the presence of a well-ordered condensed phase at lower temperatures suggest that these interactions are *attractive*.

### B. Xe binding and lateral interaction

More about the binding energy of Xe on Pd(111) and the lateral interactions can be learned from the TPD experiments presented in Sec. III D and Fig. 6. The desorption energy $E^0_{des} = 320$ meV, inferred from the $\sqrt{3}$ peak in Fig. 6(b), should be compared to the Xe binding energy range of 360–330 meV reported by Wandelt and Hulse.[6] Note that the latter values were determined from a Redhead analysis *assuming* a prefactor of $\nu_0 = 10^{15}$ Hz; taking a prefactor between $10^{12}$ and $10^{13}$ Hz as determined from Fig. 6(b) would give about 50 meV smaller values for $E^0_{des}$. In contrast to Wandelt and Hulse, we do not find any significant decrease of the binding energy up to the saturation coverage of the $(\sqrt{3}\times\sqrt{3})R30°$ phase. Only upon compression of the commensurate Xe layer is this energy strongly reduced. From the position of the 'HI, HIR' peak in Fig. 6 at about 95 K we can estimate the binding energy of the Xe atoms incorporated in the dense domain walls to be of the order of 250 meV, which is about 70 meV smaller than in the commensurate $(\sqrt{3}\times\sqrt{3})R30°$ domains. Note that this low-temperature desorption peak, as well as the corresponding compressed HI and HIR phases, have not been detected by Wandelt and Hulse,[6] because their adsorption and desorption experiments were performed above 95 K, where only the $(\sqrt{3}\times\sqrt{3})R30°$ phase is stable.

The strict *first-order* desorption behavior up to saturation of the $(\sqrt{3}\times\sqrt{3})R30°$ phase is again indicative of *weak* lateral interactions. Here ''weak'' means that the lateral interaction energy per atom $V_{lat}$ is small compared to the thermal energy $k_BT$ in the temperature range $T = 100$–$120$ K, where the desorption takes place,[34] i.e., $V_{lat} \ll 10$ meV. In fact, *attractive* interactions $\gtrsim k_BT$ would stabilize the phase coexistence between a 2D gas and a 2D solid phase, resulting in a zero-order desorption behavior characterized by a common leading edge of the TPD traces. On the other hand, sizable *repulsive* interactions would give rise to a second-order-like character, namely, a shift of the desorption maxima towards lower temperature with increasing initial coverage.[35] To further illustrate this point, we may compare the present findings with the Xe desorption on Pt(111).[36] In this case, the desorption from the $(\sqrt{3}\times\sqrt{3})R30°$ phase occurs at around 105 K via a process which is zero order for higher initial coverages but first order at low Xe coverages. Despite the rather limited first-order regime for the Xe/Pt(111) system, a quantitative fit of the desorption curves can only be obtained by assuming a very small (effective) lateral interaction of $3\times 7$ meV$= 21$ meV only.[35,36] By comparison, the lateral interaction in the case of Xe/Pd(111), where the first-order behavior is much more pronounced, should be significantly smaller.

The stronger binding of Xe to the Pd(111) surface ($\sim$320 meV) as compared to Pt(111) [$\sim$260 meV (Ref. 35)] is somewhat surprising, since the van der Waals interaction between Xe and metals with a very similar free electron density such as Pt and Pd should not be too different. However, in contrast to Pd, the (111) face of Pt supports an *sp* surface state or resonance close to the Fermi level in the center of the surface Brillouin zone.[37] On Pt(111) the surface state is partially occupied, whereas on Pd(111) it is not. The contribution of intrinsic surface states to the binding of the noble gases on metals has been proposed to explain the stronger *vertical* binding of Xe on Pd(111) as compared to Pt(111) and (at least partially) the stronger repulsive contribution to the *lateral* interactions for the Xe/Pd(111) system.[38] A stronger Xe-metal binding was also found to correlate with a larger Xe-induced work function change, i.e., with an increase of the adsorption-induced dipole moment.[6] Therefore, an enhanced repulsive contribution to the lateral interaction for strongly binding substrates is also expected to arise from the related increase of the Xe dipole-dipole repulsion.[6,17]

In summary, we can understand the weak *effective* lateral interactions in the Xe $(\sqrt{3}\times\sqrt{3})R30°$ phase (evidenced by the first order character of the corresponding TPD spectra in Fig. 6) to arise from an almost complete canceling of the attractive van der Waals interaction between neighboring Xe atoms by the strong repulsive contributions to the lateral interaction, expected for a strongly binding substrate such as Pd(111). On the other hand, the formation of 2D islands (see discussion in Sec. IV A) suggests that the attractive van der Waals contribution is not completely canceled (or even overcompensated as suggested in Refs. 6 and 7) by the repulsive contributions. Thus the net, *effective* lateral interaction is certainly weak but probably still attractive on the *clean* Pd(111) surface.

Note, that the observation of a ''dilute'' phase at temperatures above 80 K (Refs. 7 and 12) are not necessarily in contradiction with the presence of *weak* lateral attractions and hence the formation of 2D islands or clusters as observed at *lower* surface temperatures. Indeed, the disappearance of the sharp (1/3,1/3) LEED spots (Fig. 7) is indicative of a thermally induced disordering (2D melting or sublimation) of the weakly bound 2D solid phase. Likewise, the first-order

desorption indicates that the $(\sqrt{3}\times\sqrt{3})R30°$ phase dissolves into a single, weakly correlated phase (to be identified with the ''dilute'' phase of Refs. 7 and 12) well below the onset of desorption at $T\approx 110$ K (Fig. 6). Quantitative information on the size of the lateral interactions could be obtained in a high resolution LEED study of the coverage and temperature dependence of the structural ordering within the $(\sqrt{3}\times\sqrt{3})R30°$ phase.

### C. The influence of impurities

The amplitude and sign of the lateral interactions could depend on the cleanliness, i.e., on the presence of impurities and/or surface defects. For instance, an increase of the binding energy at a surface defect or impurity could increase the repulsive contribution to the lateral interaction, as was observed for Xe atoms adsorbed at the step edges on a Pt(111) surface.[17] This is particularly problematic in the present case, since the lateral interactions on the clean Pd(111) surfaces are quite weak and a possible modification could give rise to large *relative* changes or even a reversal of the sign. As a consequence, the shape of the desorption spectra and the structural phase diagram can be significantly affected. Such a strong influence of the presence of surface impurities like H and CO is, indeed, observed experimentally.[22]

One example concerns the Xe adlayer structure at monolayer saturation. Whereas the clean surface yields the 6 spot LEED pattern [Fig. 2(e)], a slight hydrogen contamination gives rise to a completely different LEED pattern characterized by a spot splitting into three spots forming a triangle pointing *inward* [Fig. 5(b)]. At first sight, the Xe adlayer in this phase appears to be nonrotated with respect to the high symmetry directions of the substrate. In fact, the position of the satellite spots is close to that expected for a $(7\times 7)$ phase. A very similar spot splitting was reported for $D_2$ adsorbed on graphite[39] and has been interpreted as an incommensurate structure (termed the $\gamma$ phase) in which the adlayer is rotated in such a way that the modulation or buckling giving rise to the satellite spots is exactly aligned with the substrate. If we attribute the LEED pattern in Fig. 5(b) to such a $\gamma$ phase, we can determine from the spot splitting the Xe coverage to $0.40\pm 0.01$ and the rotation angle of the adlayer to $(22.2\pm 1)°$ [Fig. 5(c)].

As a result, we suggest that the main effect of a contamination of the Pd(111) surface is a change of the monolayer saturation coverage $\Theta_{ML}$ and a modification of the adlayer rotation. Both effects can be attributed to a change of the lateral interactions since this would affect the compressibility of the adlayer and, hence, the saturation coverage as well as the elastic properties (stiffness) of the monolayer, thereby affecting its rotational behavior.[32] Also the previously observed high-order commensurate phases[7,12] $(\sqrt{19}\times\sqrt{19})R23.4°(\Theta_{ML}=0.37)$ and $(\sqrt{7}\times\sqrt{7})R19.2°(\Theta_{ML}=0.43)$, which we attribute to contamination with H and CO, respectively,[22] can be understood along the same lines. These phases again differ in the saturation coverage as well as in the rotation angle.

## V. CONCLUSION

We have studied the adsorption and structure formation of Xe on the clean Pd(111) surface. We find a strong binding to the substrate $(320\pm 10$ meV) but a very weak (probably attractive) effective lateral interaction, which is definitely smaller than $k_BT$ at desorption temperatures, i.e., $V_{lat}\ll 10$ meV. Within the monolayer regime, a phase transition sequence $(\sqrt{3}\times\sqrt{3})R30°\rightarrow$HI$\rightarrow$HIR is observed, which is consistent with theory and similar to the case of Kr on graphite. The $(\sqrt{3}\times\sqrt{3})R30°$ phase is stable at low temperature but may dissolve into a weakly correlated (''dilute'') phase at higher temperature—again suggesting *weak* attractive Xe-Xe interactions. The Xe adlayer structure is very sensitive to the presence of impurities, such as H and CO. This sensitivity is attributed to the weak effective lateral interaction and the strong relative changes of the amplitude and, possibly, even the sign of $V_{lat}$.

## ACKNOWLEDGMENT

This work was financially supported by the Austrian Science Foundation (FWF) under Contract No. P13841-CHE.

*Present address: Institut für Physikalische und Theoretische Chemie, Universität Erlangen-Nürnberg, D-91058 Erlangen, Germany.

†Present address: Ellcotec, Auerbach 16/11, A-5301 Eugendorf, Austria.

‡Present address: Institut für Halbleiter- und Festkörperphysik, Johannes Kepler Universität Linz, A-4040 Linz, Austria.

§Electronic address: zeppenfeld@exphys.uni-linz.ac.at

[1] M. Bienfait, *Noble Gases on Graphite, Lamellar halides, MgO, and NaCl*, Landolt Börnstein New Series III/42-A1 (Springer Verlag, Berlin, 2001), p. 117.

[2] P. Zeppenfeld, *Noble Gases on Metals and Semiconductors*, Landolt Börnstein New Series III/42-A1 (Springer Verlag, Berlin, 2001), p. 67.

[3] L.W. Bruch, M.W. Cole, and E. Zaremba, *Physical Adsorption: Forces and Phenomena* (Clarendon, Oxford, 1997).

[4] J.R. Chen and R. Gomer, Surf. Sci. **94**, 456 (1980).

[5] K. Christmann and J.E. Demuth, Surf. Sci. **120**, 291 (1982).

[6] K. Wandelt and J.E. Hulse, J. Chem. Phys. **80**, 1340 (1984).

[7] B. Vogt, B. Kessler, N. Müller, G. Schönhense, B. Schmiedeskamp, and U. Heinzmann, Phys. Rev. Lett. **67**, 1318 (1991).

[8] N.D. Lang, Phys. Rev. Lett. **46**, 842 (1981).

[9] J.E. Müller, Phys. Rev. Lett. **65**, 3021 (1990).

[10] J.L.F. Da Silva, C. Stampfl, and M. Scheffler, Phys. Rev. Lett. **90**, 066104 (2003).

[11] P. Zeppenfeld, U. Becher, K. Kern, and G. Comsa, J. Electron Spectrosc. Relat. Phenom. **54-55**, 265 (1990).

[12] G. Hilgers, M. Potthoff, N. Müller, and U. Heinzmann, Surf. Sci. **322**, 207 (1995).

[13] M. Caragiu, Th. Seyller, and R.D. Diehl, Phys. Rev. B **66**, 195411 (2002).

[14] Th. Seyller, M. Caragiu, R.D. Diehl, P. Kaukasoina, and M. Lindroos, Chem. Phys. Lett. **291**, 567 (1998).

[15] B. Narloch and D. Menzel, Chem. Phys. Lett. **270**, 163 (1997); Surf. Sci. **412**, 562 (1998).
[16] Th. Seyller, M. Caragiu, R.D. Diehl, P. Kaukasoina, and M. Lindroos, Phys. Rev. B **60**, 11 084 (1999).
[17] P. Zeppenfeld, S. Horch, and G. Comsa, Phys. Rev. Lett. **73**, 1259 (1994).
[18] S. Horch, P. Zeppenfeld, and G. Comsa, Appl. Phys. A **60**, 147 (1995).
[19] G. Hilgers, Ph.D. thesis, University of Bielefeld (1992).
[20] B. Kessler, N. Müller, B. Schiedeskamp, B. Vogt, and U. Heinzmann, Z. Phys. D: At., Mol. Clusters **17**, 11 (1990).
[21] B. Kessler, N. Müller, B. Schiedeskamp, B. Vogt, and U. Heinzmann, Phys. Scr. **41**, 953 (1990).
[22] J.F. Zhu, H. Ellmer, H. Malissa, Th. Brandstetter, D. Semrad, and P. Zeppenfeld (unpublished).
[23] R. David, K. Kern, P. Zeppenfeld, and G. Comsa, Rev. Sci. Instrum. **57**, 2771 (1986).
[24] Physikalische Instrumente, Dr. H. Schlichting, D-82205 Gilching, Germany.
[25] P. Zeppenfeld, K. Kern, R. David, and G. Comsa, Phys. Rev. B **38**, 3918 (1988).
[26] M. Nielsen, J. Als-Nielsen, J. Bohr, and J.P. McTague, Phys. Rev. Lett. **47**, 582 (1981).
[27] H. Schlichting and D. Menzel, Surf. Sci. **272**, 27 (1992); Rev. Sci. Instrum. **64**, 2013 (1993).
[28] M.D. Chinn and S.C. Fain, Phys. Rev. Lett. **39**, 146 (1977); S.C. Fain, M.D. Chinn, and R.D. Diehl, Phys. Rev. B **21**, 4170 (1980).
[29] E.D. Specht, A. Mak, C. Peters, M. Sutton, R.J. Birgeneau, K.L. D'Amico, D.E. Moncton, S.E. Nagler, and P.M. Horn, Z. Phys. B: Condens. Matter **69**, 69 (1987) and references therein.
[30] K. Kern, Phys. Rev. B **35**, 8265 (1987).
[31] T. Halpin-Healy and M. Kardar, Phys. Rev. B **31**, 1664 (1985).
[32] A.D. Novaco and J.P. McTague, Phys. Rev. Lett. **38**, 1286 (1977); J.P. McTague and A.D. Novaco, Phys. Rev. B **19**, 5299 (1979).
[33] As mentioned in Sec. III C, the presence of a ''dilute'' phase appears to be promoted by the presence of surfaces impurities, most likely hydrogen. Therefore, the critical temperature for the transition from an ordered $(\sqrt{3}\times\sqrt{3})R30°$ phase to a disordered 2D gas or liquid phase could also be strongly affected by the presence of impurities and should be regarded with great caution.
[34] B. Lehner, M. Hohage, and P. Zeppenfeld, Chem. Phys. Lett. **369**, 275 (2003).
[35] B. Lehner, M. Hohage, and P. Zeppenfeld, Phys. Rev. B **65**, 165407 (2002).
[36] W. Widdra, P. Trischberger, W. Frieß, D. Menzel, S.H. Payne, and H.J. Kreuzer, Phys. Rev. B **57**, 4111 (1998).
[37] P. Roos, E. Bertel, and K.D. Rendulic, Chem. Phys. Lett. **232**, 537 (1995).
[38] E. Bertel, Surf. Sci. **367**, L61 (1996).
[39] J. Cui and S.C. Fain, Phys. Rev. B **39**, 8628 (1989).